Journal of Alloys and Compounds 507 (2010) 146–150

Contents lists available at ScienceDirect

Journal of Alloys and Compounds

journal homepage: www.elsevier.com/locate/jallcom

Sintering and microstructure evolution of columnar nickel-based superalloy sheets prepared by EB-PVD

S. Chen*, S.J. Qu, J. Liang, J.C. Han

Center for Composite Materials, Harbin Institute of Technology, P.O. Box 3010, Harbin 150001, PR China

ARTICLE INFO

Article history:
Received 10 March 2010
Received in revised form 19 July 2010
Accepted 20 July 2010
Available online 29 July 2010

Keywords:
Nickel-based superalloy
EB-PVD
Columnar structure
Sintering
Mechanical properties

ABSTRACT

A ~0.15 mm-thick columnar nickel-based superalloy sheet was obtained by electron beam physical vapor deposition (EB-PVD). The as-deposited alloy sheet was sintered at different conditions. The microstructure of the specimens before and after sintering was characterized by using scanning electron microscopy. An X'Pert texture facility was used to determine the crystallographic orientation of the as-deposited alloy sheet. The phase transformation was investigated by X-ray diffraction. Tensile tests were conducted at room temperature on as-deposited and sintered specimens. The results show that the as-deposited sheet is composed of typical columnar structures. After sintering, however, the columnar structure degrades. The degradation depends on sintering temperature and time. Both the ultimate tensile strength and the elongation percentage are effectively improved after sintering.

1. Introduction

Electron beam physical vapor deposition (EB-PVD) is a high-efficiency and non-equilibrium deposition technique [1]. It is commonly used to deposit thermal barrier coatings (TBCs) on rotating blades and some high-pressure turbine section vanes, which require surfaces with a smooth finish and the ability to withstand high thermo-mechanical strain [2–5]. The unique columnar microstructure is typical of TBCs obtained by EB-PVD. The loosely bonded columnar grains provide outstanding resistance against thermal shock and mechanical strains, which are associated with high-temperature, high-pressure turbine blades [6]. Recently, a significant amount of research work has been conducted on the application of EB-PVD technology in the production of microlaminate material [7] and thin alloy sheets. He et al. reported on oxide dispersion strengthened (ODS) Ni-based superalloy foils produced by EB-PVD [8]. Chen et al. studied the microstructure and mechanical properties of Ni-based superalloy foil with nanocrystalline surface layer produced by EB-PVD [9]. Li et al. investigated the isothermal oxidation behaviors of Ni-based alloy sheets produced by EB-PVD [10]. In these studies, columnar structures were obtained. These structures significantly affected the mechanical properties of alloy sheets. The ultimate tensile strength and elongation percentage of as-deposited alloy sheets were small because of cracks propagating along the interface of columnar grains. Therefore, to understand the full potential and performance benefits offered by EB-PVD, it is necessary to reduce the effects of columnar structures on the mechanical properties. Earlier studies have examined the effects of sintering on the properties of the topcoat. Some researches have been done to reveal the mechanisms underlying topcoat sintering and the associated changes in coating microstructure [11,12]. Guo et al. reported that the columnar structure of a 4.0 mol% Y_2O_3 partially stabilized ZrO_2 coating material degraded after thermal exposure, and both hardness and Young's modulus significantly increased [13]. Similar results in an 8 wt% Y_2O_3 partially stabilized ZrO_2 coating material were also reported by Wellman et al. [14]. These studies are essential to correlate sintering-related changes in the topcoat to coating failure. However, this kind of research has seldom been done for EB-PVD thin alloy sheets.

In the present study, a Ni-based superalloy sheet with a typical columnar structure was prepared by EB-PVD. The microstructural evolution and tensile properties of the alloy sheet before and after sintering in vacuum were investigated.

2. Experimental

A large-scale EB-PVD equipment (GEKONT L5) was employed to prepare a Ni-based superalloy sheet. A Y_2O_3 ingot and a Ni–20Cr–1.4Al (wt%) ingot were selected as vapor sources. Deposition was performed under high vacuum (1×10^{-3} Pa) using a turbo-molecular pump. During preparation, the deposition rate was adjusted by changing the currents of the electron beams. The deposition speed was ~3 μm/min

* Corresponding author at: Center for Composite Materials, Harbin Institute of Technology, P.O. Box 3010, Harbin 150001, PR China. Tel.: +86 0451 86402432; fax: +86 0451 86412236.
E-mail address: s.chen_hit@163.com (S. Chen).

0925-8388/$ – see front matter © 2010 Elsevier B.V. All rights reserved.
doi:10.1016/j.jallcom.2010.07.142

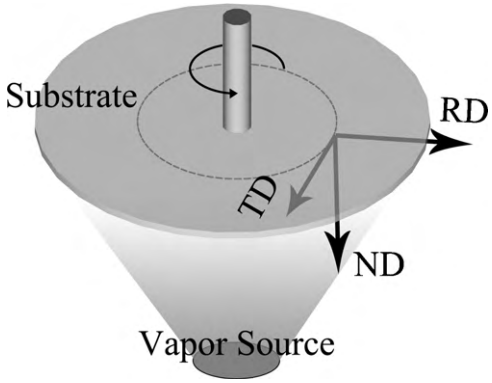

Fig. 1. Illustration of the local rectangular coordinate system on specimens.

and the total deposition time was 50 min. The rotation speed was 12 rpm and the substrate temperature was 720 °C, with a 20 °C error range. After deposition, the Ni-based superalloy sheet was mechanically stripped away from the stainless steel substrate. The as-deposited samples were then sintered at 760 °C for 3 h, 760 °C for 20 h and 1050 °C for 3 h. Prior to sintering, samples were encapsulated in quartz tubes and evacuated to less than 1×10^{-3} Pa.

Microstructural investigations of as-deposited and sintered specimens were performed by scanning electron microscopy (SEM) and X-ray diffraction (XRD). The chemical composition of the alloy sheet was determined by X-ray fluorescence spectrometry (XRF). Pole figures were obtained using a PANalytical X'Pert Pro diffractometer using Cu radiation with a nickel filter in the diffracted beam. Textural data were collected to a psi angle of 70° and corrected for contributions from the background and for defocusing. Data were then analyzed using a PANalytical X'Pert texture software in order to produce complete pole figures for the crystallographic orientation type. The reference frame is illustrated in Fig. 1. The radius direction, tangent direction, and normal direction were denoted as RD, TD and ND, respectively.

Tensile tests were conducted at room temperature on as-deposited and sintered specimens. The sample size and shape in the tensile tests are shown in Fig. 2. Specimens were strained at a rate of approximately 0.02 s^{-1} with an extensometer clipped to the gauge length until failure.

3. Results and discussion

3.1. Microstructures

A Ni–18Cr–0.6Al superalloy sheet strengthened with 0.4Y_2O_3 (wt%) was deposited. The thickness of the sheet is ~150 μm.

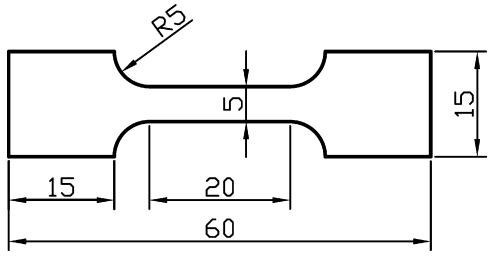

Fig. 2. Sample size and shape in tensile tests.

Fig. 3(a) shows the cross-sectional morphology (fracture surface) of the as-deposited sheet. Molecules of the vapor flow with a certain kinetic energy, when they collide with the condensation surface, go into an adsorbed state and exchange the energy with surface atoms, and move jump-like over the surface. The surface temperature determines the level of thermal activation of the adsorbed atom, number of jumps, probability of collision, interaction with other adsorbed atoms, and formation of their respective atomic configurations. According to an experimentally established schematic of structural zones [15], substrate temperature (T_s) is one of the main parameters that determine the structure of thick condensates. When $T_s/T_m < 0.3$ (T_m is the melting temperature of condensates in K), an amorphous or nanosize structure is formed. In the second high-temperature zone ($0.3 < T_s/T_m < 0.5$), condensates are characterized by a columnar structure with a predominantly crystallographic orientation. In the third high-temperature zone ($T_s/T_m > 0.5$), the columnar structure gradually changes to an equiaxial grain structure. T_s/T_m in this study belongs to the third temperature zone. However, as can be seen in Fig. 3(a), a typical columnar structure is formed. This is caused by the addition of Y_2O_3 in the condensate since Y_2O_3 can effectively inhibit grain growth in the matrix by pinning grain boundaries [16]. The surface morphology of the as-deposited alloy sheet is shown in Fig. 3(b) and (c). The terminal faces on top of the columns exhibit a pyramidal shape. At first glance, they look like octahedral planes on crystals with a cubic symmetry. It can be seen from Fig. 3(c) that each pyramidal tip corresponds to a columnar grain. Cracks can easily propagate along the interface of the columnar grain.

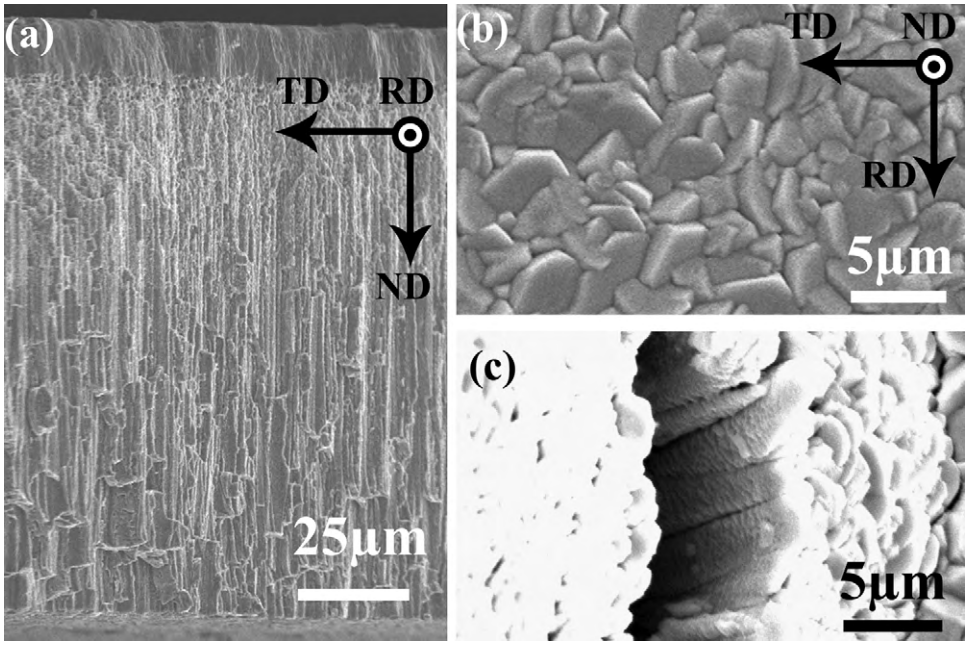

Fig. 3. SEM micrographs of the as-deposited Ni-based superalloy sheet: (a) cross-sectional morphology, (b) top surface and (c) crack on the top surface.

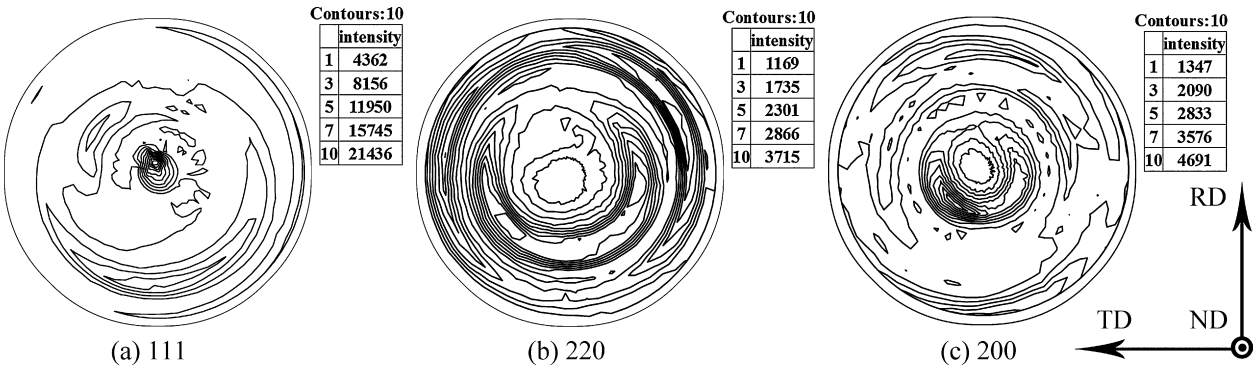

Fig. 4. (1 1 1), (2 2 0), and (2 0 0) pole figures of the as-deposited specimen.

A recent work suggests that the growing columns obtained by EB-PVD have a certain crystallographic orientation. Vapor deposition has also been reported to result in the preferential growth of condensates [17]. This preferential growth causes crystallographic texture, which has been explained by 'evolutionary selection' [17,18]. The theory of 'evolutionary selection' states that the crystal with the fastest growing direction orients itself towards the vapor source. Fig. 4 shows the typical (1 1 1), (2 2 0), and (2 0 0) pole figures of the as-deposited alloy sheet. The (1 1 1) plane is nearly parallel to the substrate surface, but the poles of (2 2 0), and (2 0 0) are distributed around the apex of the figure in an approximately circular fashion. This result suggests that a predominantly ⟨1 1 1⟩ fiber texture is formed. A number of different textures in EB-PVD coatings, e.g., ⟨0 0 1⟩, ⟨0 1 1⟩, ⟨1 1 3⟩ and ⟨1 1 1⟩-type textures, were found on rotated and stationary substrates [19–21]. Factors, such as vapor incidence angle (VIA), substrate temperature, condensate thickness and substrate rotation, influence the texture of EB-PVD condensates. However, no clear relationship has been established by far.

The cross-sectional (fracture surface) and surface morphologies of samples sintered at 760 °C for 3 and 20 h are shown in Fig. 5(a)–(c). It can be found that the cross-sectional and surface morphologies of sintered samples change significantly. Fig. 5(a) presents the sintering of the columnar structure and the grain boundaries being reformed effectively. It should also be noted that, in the middle part of the cross-section, traces of columnar structure can still be found. However, there are no signs of columnar structures in samples treated at 760 °C for 20 h [Fig. 5(b)]. This indicates that, under this temperature, the kinetic energy of condensate atoms is still limited. Sintering only occurs at the interface of the columns and depends on heating time. Therefore, the grain size does not change under this condition. The effect of sintering is also observed on the surface morphology. There is almost no difference of the surface morphology between samples sintered for 3 and 20 h. Therefore, only one image of the surface is given in Fig. 5(c). The pyramidal tips, which are a distinctive feature of as-deposited sheets, are no longer evident after sintering. A mud-crack-like shape is observed, which presents the effect of sintering on the samples.

Fig. 6 shows the morphologies of the samples treated at 1050 °C for 3 h. After being treated at a higher temperature (1050 °C), the cross-sectional morphologies of the samples show more obvious signs of sintering [Fig. 6(a)]. The previous, evident columnar structures completely disappear under this treatment. From Fig. 6(b), some new precipitates can be observed on the surface of the treated samples. This indicates that recrystallization may have occurred under this condition. Grain growth seems to be very significant during the sintering procedure.

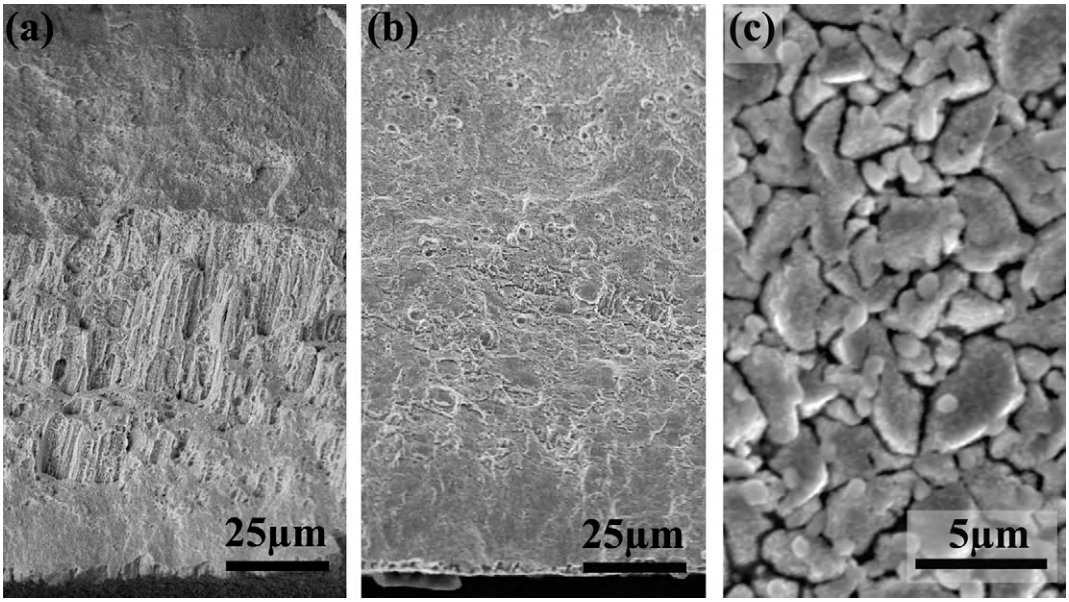

Fig. 5. SEM micrographs of the sintered samples: cross-sectional morphologies of samples treated at (a) 760 °C for 3 h, (b) 760 °C for 20 h and (c) top surface.

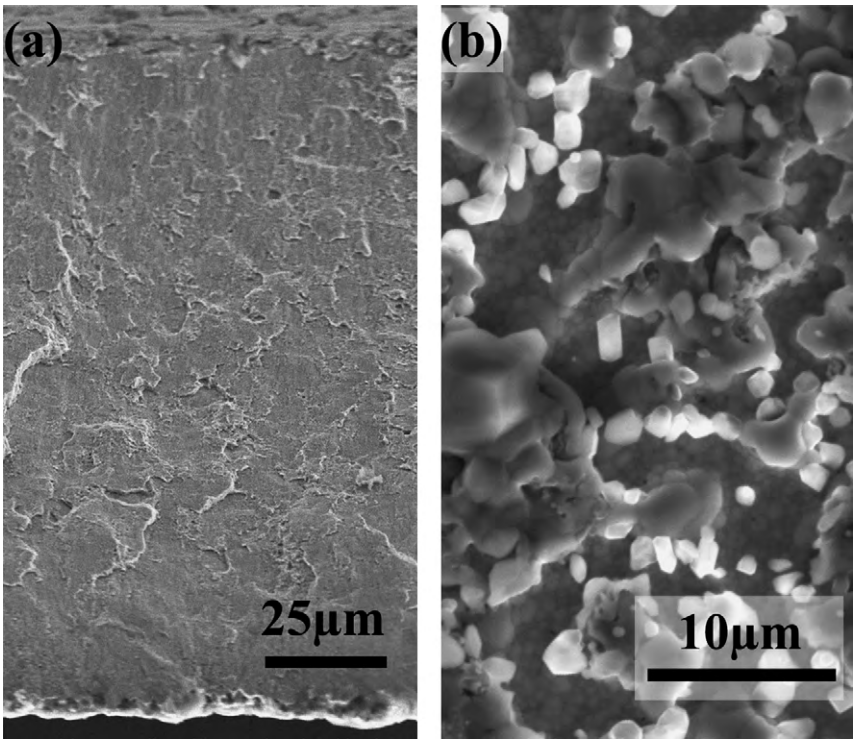

Fig. 6. SEM images of the samples sintered at 1050 °C: (a) cross-sectional morphology and (b) top surface.

3.2. X-ray analysis

The XRD patterns of as-deposited and heat-treated samples are shown in Fig. 7. S1, S2, and S3 in Fig. 7 are referred to as as-deposited samples and samples treated at 760 and 1050 °C, respectively. The XRD pattern reveals that the main phase of the alloy is γ-Ni and that no phase transition occurs before and after sintering. However, the diffraction peaks of the treated samples are relatively stronger and narrower than the as-deposited sample. This indicates that the degree of crystallization of the treated samples has been elevated by heat treatments. Furthermore, the diffraction peaks, especially (2 2 0), (3 1 1), and (2 2 2) of samples treated at 1050 °C, shifted to smaller angles compared to as-deposited samples and samples treated at 760 °C. This result suggests that the inter-planar spacing of γ-Ni is enlarged according to Bragg's equation. EB-PVD is a high-efficiency and non-equilibrium deposition procedure. During the procedure, some atoms, such as Al and Cr, cannot attain the equilibrium position. Therefore, these atoms exist as free elements. When the condensate is heated at high temperature, free atoms will dissolve in the nickel matrix and the inter-planar spacing of the matrix will be enlarged by the solid solution.

3.3. Tensile properties

Tensile properties of samples before and after sintering are shown in Fig. 8. The elongation percentage of heat-treated samples all significantly increases compared to the as-deposited samples, whereas the tensile strength increases to 1220 MPa (for samples treated at 760 °C) and then decreases to 960 MPa (for samples

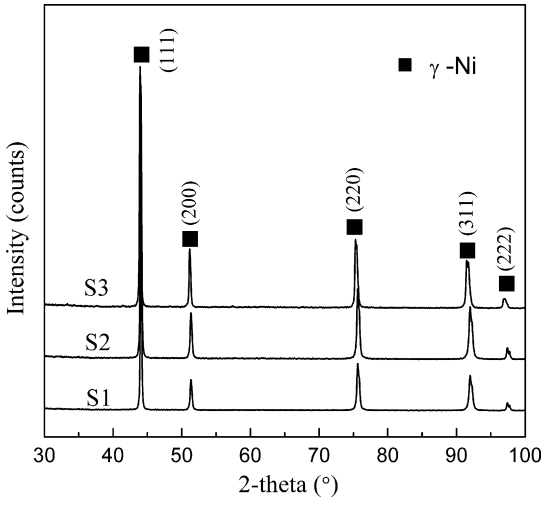

Fig. 7. XRD patterns of the alloy sheet before and after sintering.

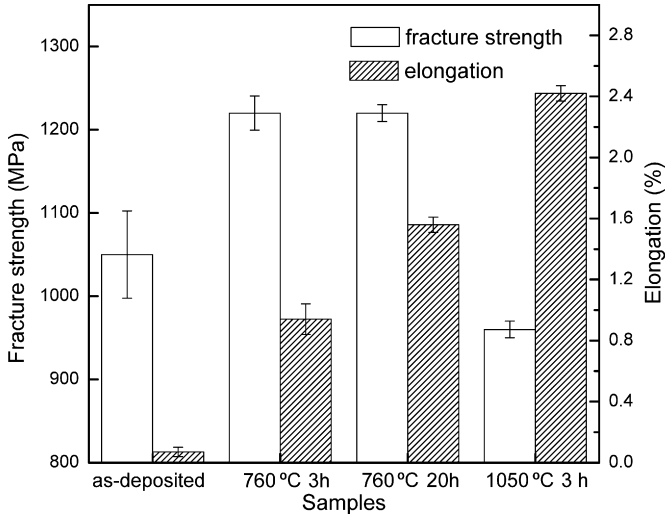

Fig. 8. Tensile strength and elongation of the alloy sheet before and after sintering.

treated at 1050 °C). In Fig. 3(a), the fracture of the as-deposited sample is a typical brittle inter-granular fracture pattern. The tensile strength is 1060 MPa with an 80 MPa error range, and the elongation percentage is only 0.07%. The poor ductility is caused by the weak connection between the columnar grains. The large error range in strength suggests that, during the non-equilibrium deposition procedure, a non-homogeneous microstructure is obtained. After sintering at 760 °C, the grain boundary conditions are significantly improved. Therefore, both the strength and elongation percentage of the samples are significantly increased. After sintering for 20 h, individual columns disappear completely. The elongation percentage of samples treated for 20 h is higher than that of samples treated for 3 h. For samples treated at 1050 °C, the reduction in strength is caused by grain growth during sintering according to Hall–Petch relationship. Grain growth and recrystallization result in multiple-slip systems. From the fracture surface morphologies [Fig. 6(a)], the fracture mode of the samples changes from a brittle inter-granular fracture [Fig. 3(a)] to a ductile dimple pattern, indicating that the ductility of the samples was improved significantly. The elongation percentage of the samples reaches the maximum value of 2.4%.

4. Conclusions

A ~0.15 mm-thick columnar nickel-based superalloy sheet was obtained by EB-PVD. A typical columnar structure was formed with a predominantly ⟨1 1 1⟩ fiber texture. The main phase of the alloy sheet is γ-Ni. After sintering, no phase transition can be detected. The columnar structure degrades, depending on sintering temperature and time. The as-deposited sheet presents poor ductility because of the weak connection between the columnar grains. The ultimate tensile strength and elongation percentage are 1060 MPa and 0.07%, respectively. After sintering at 760 °C for 3 h, the ultimate tensile strength and elongation percentage of the sheet increase to 1220 MPa and 0.94%, respectively. With the sintering time increases to 20 h, the elongation percentage increases to 1.42%. For samples are sintered at 1050 °C, tensile strength drops and the ductility is enhanced because of recrystallization and grain growth that resulted from sintering.

References

[1] A. Feuerstein, J. Knapp, T. Taylor, A. Ashary, A. Bolcavage, N. Hitchman, J. Therm. Spray Technol. 17 (2008) 199–213.
[2] B.-K. Jang, J. Alloys Compd. 480 (2009) 806–809.
[3] H.H. Huang, C.-C. Diao, C.-F. Yang, C.-J. Huang, J. Alloys Compd. 500 (2010) 82–86.
[4] Z.H. Xu, L.M. He, R.D. Mu, S.M. He, X.Q. Cao, J. Alloys Compd. 492 (2010) 701–705.
[5] Z.H. Xu, L.M. He, Y. Zhao, R.D. Mu, S.M. He, X.Q. Cao, J. Alloys Compd. 491 (2010) 729–736.
[6] U. Schulz, B. Saruhan, K. Fritscher, C. Leyens, Int. J. Appl. Ceram. Technol. 1 (2004) 302–315.
[7] G.D. Shi, G.Q. Chen, J. Liang, S.Y. Du, J. Alloys Compd. 476 (2009) 830–835.
[8] X.D. He, Y. Xin, M.W. Li, Y. Sun, J. Alloys Compd. 467 (2009) 347–350.
[9] S. Chen, S.J. Qu, J.C. Han, J. Alloys Compd. 484 (2009) 626–630.
[10] M.W. Li, G. Zeng, F. He, X.D. He, J. Alloys Compd. 488 (2009) L30–L34.
[11] R. Krishnamurthy, D.J. Srolovitz, Acta Mater. 57 (2009) 1035–1048.
[12] R. Krishnamurthy, D.J. Srolovitz, Mater. Sci. Eng. A 509 (2009) 46–56.
[13] S. Guo, Y. Kagawa, Ceram. Int. 32 (2006) 263–270.
[14] R.G. Wellman, H. Tourmente, S. Impey, J.R. Nicholls, Surf. Coat. Technol. 188–89 (2004) 79–84.
[15] B.A. Movchan, A.V. Demchishin, Phys. Met. Metall. 28 (1969) 83–90.
[16] D. Srinivasan, R. Corderman, R. Subramanian, Mater. Sci. Eng. A 416 (2006) 211–218.
[17] Y.H. Sohn, R.R. Biederman, R.D. Sisson, Thin Solid Films 250 (1994) 1–7.
[18] U. Schulz, S.G. Terry, C.G. Levi, Mater. Sci. Eng. A 360 (2003) 319–329.
[19] K. Wada, N. Yamaguchi, H. Matsubara, Surf. Coat. Technol. 191 (2005) 367–374.
[20] K. Wada, M. Yoshiya, N. Yamaguchi, H. Matsubara, Surf. Coat. Technol. 200 (2006) 2725–2730.
[21] U. Schulz, M. Schmucker, Mater. Sci. Eng. A 276 (2000) 1–8.